Electrical spin injection in metallic mesoscopic spin valves

Jedema, Friso

Chapter 6

Electrical detection of spin precession

6.1 Introduction

How can we study and control the behavior of the electron spin on its way from A to B in a metal or semiconductor? This is an outstanding question in the field of spintronics, where one investigates the dynamics of the electron spin during transport and explores its possibilities for new electronic applications [1–6]. Recently, electrical control of spin coherence [7] and coherent spin precession during transport [8] was studied by optical generation and detection techniques in semiconductors. Here controlled spin precession of electrically injected and detected electrons in a diffusive metallic conductor is reported, using tunnel barriers in combination with metallic ferromagnetic electrodes as spin injector and detector. The output voltage of the device is sensitive to the spin degree of freedom only, and its sign can be switched from positive to negative, depending on the relative magnetization of the ferromagnetic electrodes. It is shown that the spin direction can be controlled by inducing a coherent spin precession due to an applied perpendicular magnetic field. By inducing an average precession angle of 180 degrees, we are able to reverse the sign of the output voltage.

6.2 Polarize/analyze spin valve experiments

In the experiment a mesoscopic spin valve is used, see Fig. 6.1a , where a cobalt ferromagnetic electrode (Co1) injects spin polarized electrons into an aluminum (Al) strip via a tunnel barrier. At a distance L from the injector a second cobalt electrode (Co2) is placed, which detects spin polarized electrons in the Al strip via a tunnel barrier. The presence of the tunnel barriers is crucial as they provide a high spin dependent resistance, which

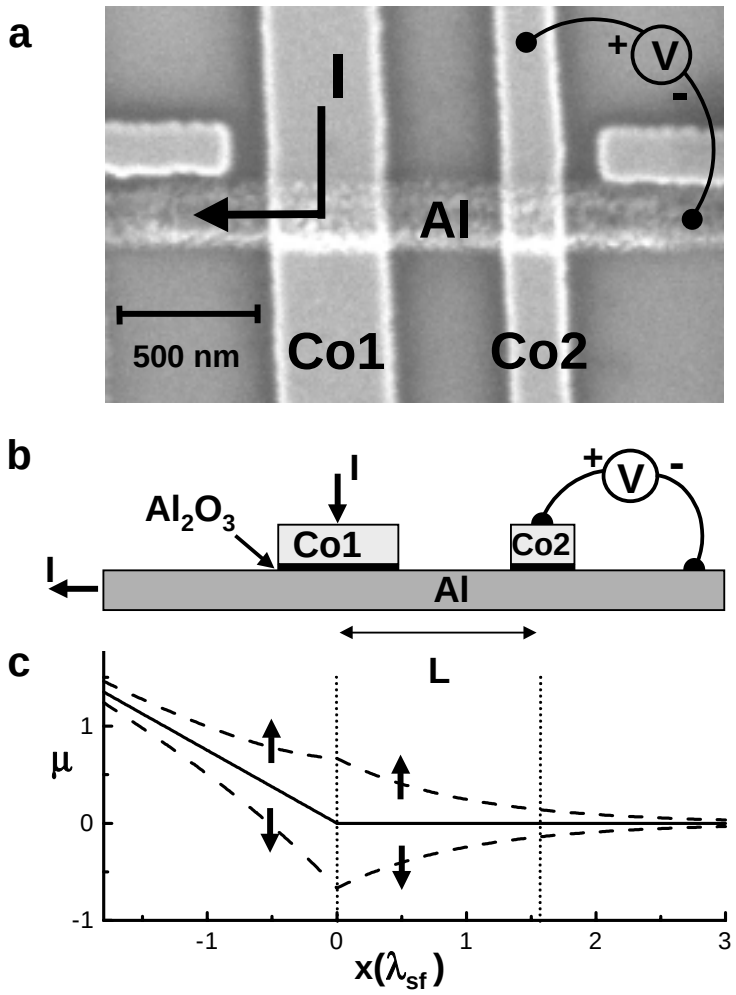

Figure 6.1: *Device Geometry. (a) Scanning electron microscope image of a device with a cobalt (Co) electrode spacing of L = 650 nm. Current is sent from Co1 into the Al strip. The voltage is measured between Co2 and the right side of the Al strip. (b) Device cross-section. (c) The spatial dependence of the spin-up and spin-down electrochemical potentials (dashed) in the Al strip. The solid lines indicate the electrochemical potential (voltage) of the electrons in the absence of spin injection.*

enhances the spin polarization of the injected current flowing into the Al strip [9–11]. In addition it causes the electrons, once injected, to have a negligible probability to lose their spin information by escaping into the Co electrodes.

During the time of flight from injector to detector, the spin direction of the electrons can therefore only be altered by (random) spin flip scattering processes in the Al strip or, in the presence of an external magnetic field, by coherent precession. In this chapter, both processes are experimentally

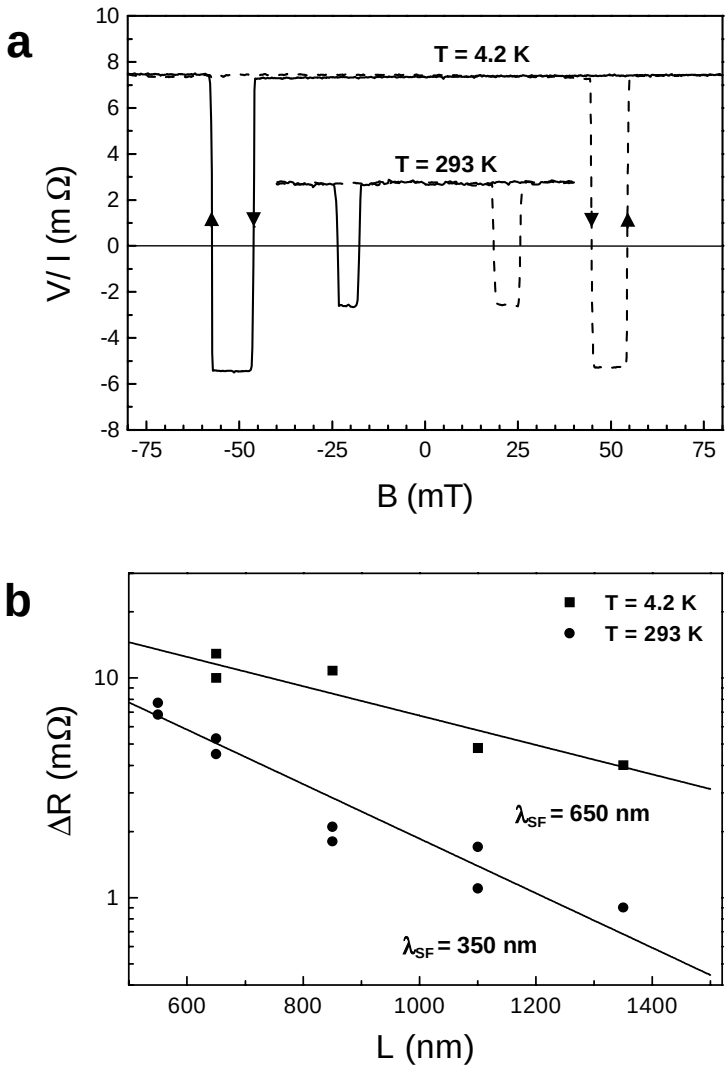

Figure 6.2: *Spin valve effect. a, Output signal (V/I) as a function of the magnetic field B, applied parallel to the long axis of the Co strips, for a sample with a Co electrode spacing L = 650 nm at T = 4.2 K and RT. The solid (dashed) lines correspond to the negative (positive) sweep direction. b, The dependence of the spin dependent resistance ΔR on the Co electrode spacing L at T=4.2 K and RT. The solid squares represent data taken at T = 4.2 K, the solid circles are taken at RT. The solid lines represent the best fits based on equation 6.1*

demonstrated by measuring the amplitude of the spin signal, first as a function of the Co electrode spacing L and secondly as a function of an applied perpendicular magnetic field. A related method to probe spin injection and detection was pioneered by Johnson and Silsbee [4]. However, the reduction of sample dimensions with 3 orders of magnitude and the introduction of tunnel barriers has increased the magnitude of the observed spin signal by

more than a million, enabling the observation of a clear sign reversal of the output voltage V due to coherent precession and has made possible an one to one comparison with theory (see Chapter 2).

Two batches of 10 and 4 devices respectively with L ranging from 550 to 1350 nm were made, using a suspended shadow mask evaporation process [12] and electron beam lithography for patterning, see Chapter 3. In the first step an Al strip with a thickness of 50 nm and a width of 250 nm, is evaporated on a thermally oxidized silicon substrate by e-gun evaporation. Next, the Al strip is exposed to an oxygen (O_2) environment of $5 \cdot 10^{-3}$ mbar for 10 minutes, producing a thin aluminum oxide (Al_2O_3) layer. In the third step, without breaking the vacuum, we evaporate two ferromagnetic Co electrodes with sizes of $0.4 \times 4\ \mu m^2$ (Co1) and $0.2 \times 12\ \mu m^2$ (Co2) and a thickness of 50 nm. Two $Al/Al_2O_3/Co$ tunnel junctions are thus formed at the overlap of the Co electrodes and the Al strip, see Fig. 6.1b. The conductivity of the Al film was measured to be $\sigma_{Al} = 1.1 \cdot 10^7\ \Omega^{-1}m^{-1}$ at room temperature (RT) and $1.7 \cdot 10^7\ \Omega^{-1}m^{-1}$ at $T = 4.2$ K. The resistance of the tunnel barriers was typically determined to be 600 Ω for the Co1 electrode and 1200 Ω for the Co2 electrode at RT, both increasing with 10 % at T = 4.2 K. Different geometric aspect ratios of Co1 and Co2 are used to obtain different coercive fields. This allows to control their relative magnetization configuration (parallel/anti-parallel), by sweeping an applied magnetic field B, directed parallel to their long axes [5, 13].

The spin polarization P of the current I injected from the Co1 electrode into the Al strip is determined by the ratio of the different spin-up and spin-down tunnel barrier resistances $R_\uparrow^{TB}$ and $R_\downarrow^{TB}$, which in first order can be written as $\frac{N_\uparrow - N_\downarrow}{N_\uparrow + N_\downarrow}$ [14–16]. Here $N_\uparrow$ ($N_\downarrow$) is the spin-up (spin-down) density of states at the Fermi level of the electrons in the Co electrodes. The injected spin current causes the densities (or electrochemical potentials) of the spin-up and spin-down electrons in the Al strip to become unequal, see Fig. 6.1c. This unbalance is transported to the Co2 detector electrode by diffusion, and can therefore be detected. Due to the spin dependent tunnel barrier resistances, the Co2 electrode detects a weighted average of the two spin densities, which causes the detected output voltage V to be proportional to P^2. Figure 6.2a shows a typical output signal (V/I) as a function of an in plane magnetic field B, directed parallel to the long axes of Co1 and Co2, taken at RT and 4.2 K. The measurements are performed by standard a.c. lock-in techniques, using a current $I = 100\ \mu A$. Sweeping the magnetic field from negative to positive, a sign reversal of the output signal is observed, when the magnetization of Co1 flips at 19 mT (RT) and 45 mT (4.2 K), and the device switches from a parallel to anti-parallel configuration. When the magnetization of Co2 flips at 25 mT (RT) and 55 mT (4.2 K),

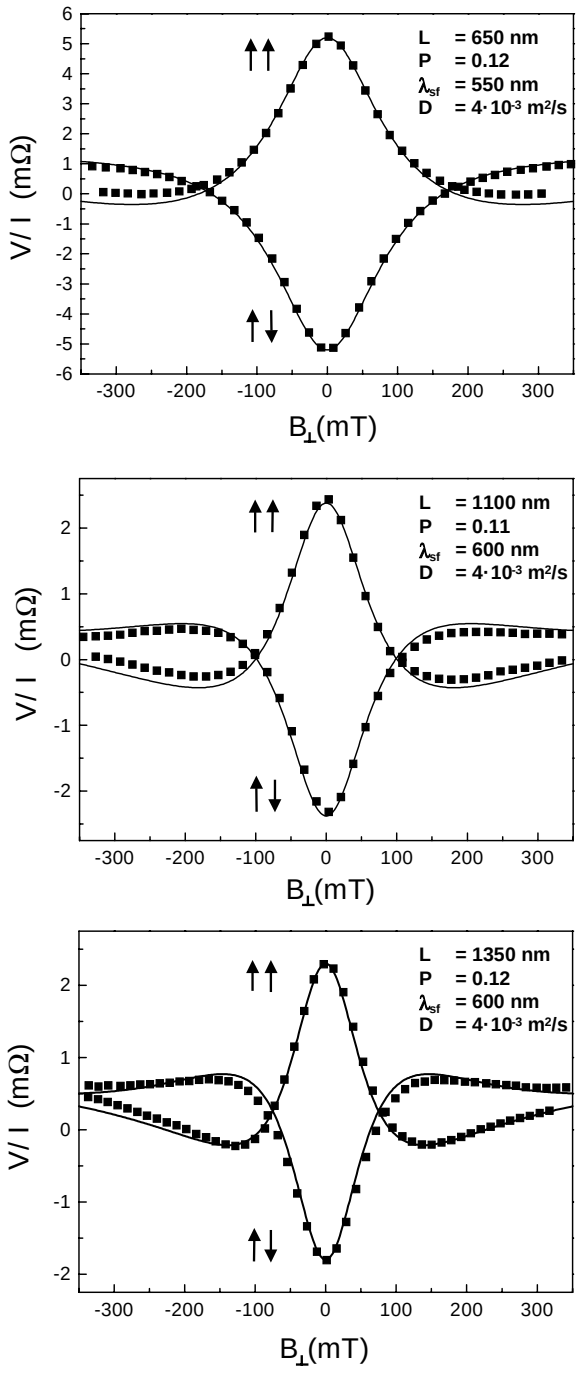

Figure 6.3: *Modulation of the output signal (V/I) due to spin precession as a function of a perpendicular magnetic field $B_\perp$, for L=650 nm, L=1100 nm and L=1350 nm. The solid squares represent data taken at T = 4.2 K, whereas the solid lines represent the best fits based on equations 6.2 and 6.3. The arrows indicate the relative magnetization configuration (parallel/anti-parallel) of the Co electrodes.*

the magnetizations are parallel again, but now point in the opposite direction. The fact that the output signal switches symmetrically around zero indicates that this experiment is sensitive to the spin degree of freedom only.

The expected magnitude of the output signal as a function of the Co electrode spacing L has been calculated in Chapter 2 by solving the spin coupled diffusion equations for the spin-up and spin-down electrons in the Al strip [17–20]. Taking into account that the tunnel barrier resistances are much larger than the resistance of the Al strip over a spin relaxation length, the expression reads:

$$\frac{V}{I} = \pm \frac{P^2 \lambda_{sf}}{2A\sigma_N} \exp(\frac{-L}{\lambda_{sf}}) \, , \tag{6.1}$$

where λ_{sf} is the spin relaxation length, A the cross-sectional area and σ_N the conductivity of the Al strip. The positive (negative) sign corresponds to a parallel (anti-parallel) magnetization configuration of the Co electrodes. Figure 6.2b shows the measured spin dependent resistance $\Delta R = \Delta V/I$ as a function of L, where ΔV is the output voltage difference between parallel and anti-parallel configuration. By fitting the data to equation 6.1 a polarization $P = 0.11 \pm 0.02$ is found at both T = 4.2 K and RT, whereas spin relaxation lengths $\lambda_{sf} = 650\pm$ 100 nm at T = 4.2 K and $\lambda_{sf} = 350\pm$ 50 nm nm at RT are obtained. The diffusion constant D is calculated using the Einstein relation $\sigma = e^2 N(E_F) D$, where e is the electron charge and $N(E_F)_{Al} = 2.4 \cdot 10^{28}$ states/eV/m^3 is the density of states of Al at the Fermi energy [21].

Using $D = 4.3 \cdot 10^{-3}$ $m^2 s^{-1}$ at T = 4.2 K and $D = 2.7 \cdot 10^{-3}$ $m^2 s^{-1}$ at RT, one obtains $\tau_{sf} = 100$ ps at T = 4.2 K and $\tau_{sf} = 45$ ps at RT. These values are in good agreement with those reported in the literature [4, 22–25]. The ratio of the phonon scattering time divided by the phonon induced spin relaxation time $a^{ph} = \tau^{ph}/\tau^{ph}_{sf}$ at RT in these Al strips are also consistent with the values obtained from the F/N/F samples with transparent contacts, as discussed in Chapter 5. For the samples discussed here one finds $a^{ph} = 1.1 \cdot 10^{-4}$, as shown in Table 5.1.

However, the obtained polarization P of around 10 % is lower than previously reported values (up to 40 %) in superconducting tunneling and TMR experiments [15, 16, 26]. Non-uniform (surface) magnetization at the Co/Al_2O_3 interface, which could lower the polarization, cannot account for this discrepancy as the full parallel spin signal is obtained at large magnetic fields as is shown in Fig. 6.5. The reduction might be related [27, 28] to a different thickness of the Al_2O_3 barrier of $\sim$ 1 nm in the spin valve samples [29] as opposed to the thicker Al_2O_3 barriers of $\sim$ 2 nm used in the experiments of Refs. [15, 16, 26].

6.3 Modulation of the spin valve signal by spin precession

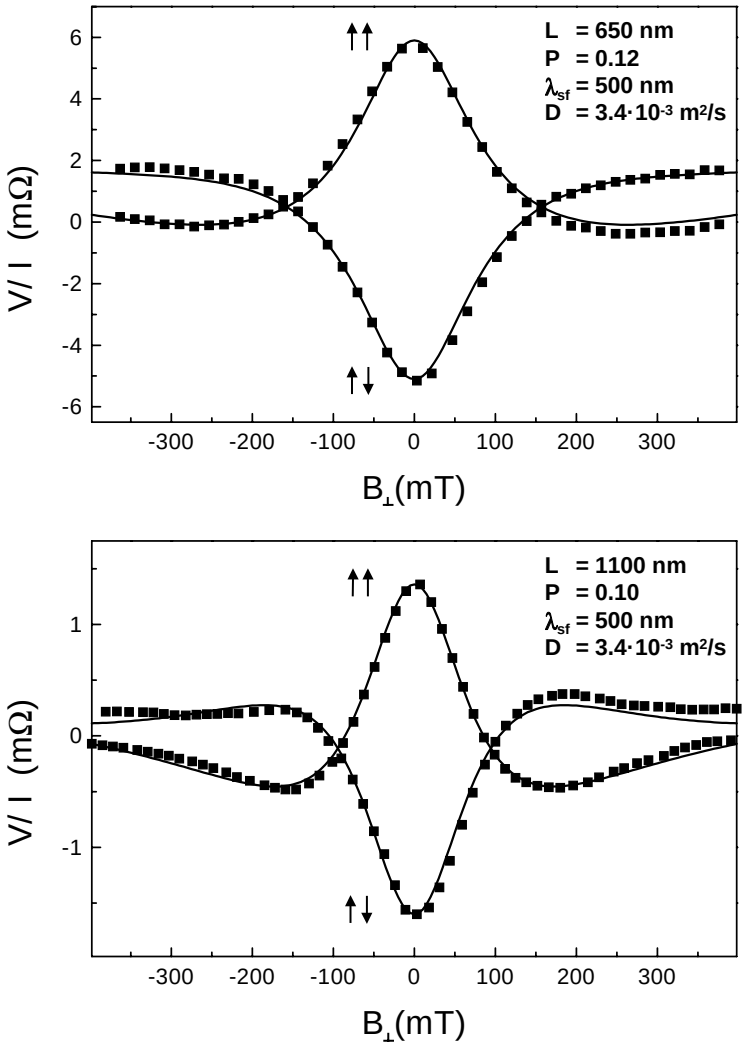

Figure 6.4: *Modulation of the output signal (V/I) due to spin precession as a function of a perpendicular magnetic field $B_\perp$, for $L = 650$ nm and $L = 1100$ nm. The solid squares represent data taken at RT, whereas the solid lines represent the best fits based on equations 6.2 and 6.3. The arrows indicate the relative magnetization configuration (parallel/anti-parallel) of the Co electrodes.*

Having determined the parameters P, λ_{sf} and D, the spin precession of the electron spin during its diffusion time t between Co1 and Co2 can be studied. In an applied field $B_\perp$, perpendicular to the substrate plane, the injected electron spins in the Al strip precess around an axis parallel to $B_\perp$ and the output voltage V at the Co2 detector electrode will be modulated

by the precession, as was derived in Chapter 2:

$$V(B_\perp) = \pm I \frac{P^2}{e^2 N(E_F)} \int_0^\infty \wp(t) \cos(\omega_l t) \exp\left(\frac{-t}{\tau_{sf}}\right) dt \ . \qquad (6.2)$$

However at large $B_\perp$, the magnetization direction of the Co electrodes is tilted out of the substrate plane with an angle ϑ. When this effect is included in the calculation one obtains:

$$V(B_\perp, \vartheta) = V(B_\perp) cos^2(\vartheta) + |V(B_\perp = 0)| sin^2(\vartheta) \ . \qquad (6.3)$$

Equation 6.3 shows that with increasing ϑ (from zero), the precession signal is reduced and a positive background output signal appears. For $\vartheta = 0$ equation 6.3 reduces to equation 6.2. In the limit that $\vartheta = \pi/2$ the magnetization of the Co electrodes is perpendicular to the substrate plane and parallel to $B_\perp$. No precession occurs anymore, and the full output signal is recovered. The angle ϑ has been determined independently as a function of $B_\perp$ by measuring the anisotropic magnetoresistance (AMR) of the Co electrodes, see Chapter 4. In Fig. 6.3 the measured output signal at T = 4.2 K is plotted as a function of $B_\perp$ for L = 650 nm, L = 1100 nm and L = 1350 nm. Prior to the measurement a magnetic field B directed parallel to the long axes of Co electrodes is used to prepare the magnetization configuration of the Co electrodes. For a parallel (anti-parallel) configuration we observe an initial positive (negative) signal, which drops in amplitude as $B_\perp$ is increased from zero field. This is called the Hanle effect in [4, 30, 31]. The two curves cross where the average angle of precession is about 90 degrees and the output signal is close to zero. As $B_\perp$ is increased beyond this field, we observe that the output signal changes sign and reaches a minimum (maximum) when the average angle of precession is about 180 degrees, thereby effectively converting the injected spin-up population into a spin-down and vice versa. The data have been fit with equations 6.2 and 6.3, as shown in Fig. 6.3. For all measured samples the best fit parameters P, λ_{sf} and D are very close to those independently obtained from the length dependence measurements, as shown in Fig. 6.2.

In Fig. 6.4 the measured output signal at RT, as a function of $B_\perp$ for L = 650 nm and L = 1100 nm. The RT temperature measurements where done with the second batch of 4 devices and had a slightly higher Al conductivity due to better alignment of two evaporation steps needed to fabricate the Al strip underneath the suspended shadow mask. The conductivity of the Al and Co strips were determined to be $\sigma_{Al} = 1.3 \cdot 10^7\ \Omega^{-1}m^{-1}$ and $\sigma_{Co} = 4.1 \cdot 10^6\ \Omega^{-1}m^{-1}$ at RT, whereas the resistance of the $Al/Al_2O_3/Co$ tunnel barriers were determined to be 800 Ω for the Co1 electrode and 2000 Ω for the Co2 electrode at RT. No measurements were performed at $T = 4.2$ K with these devices.

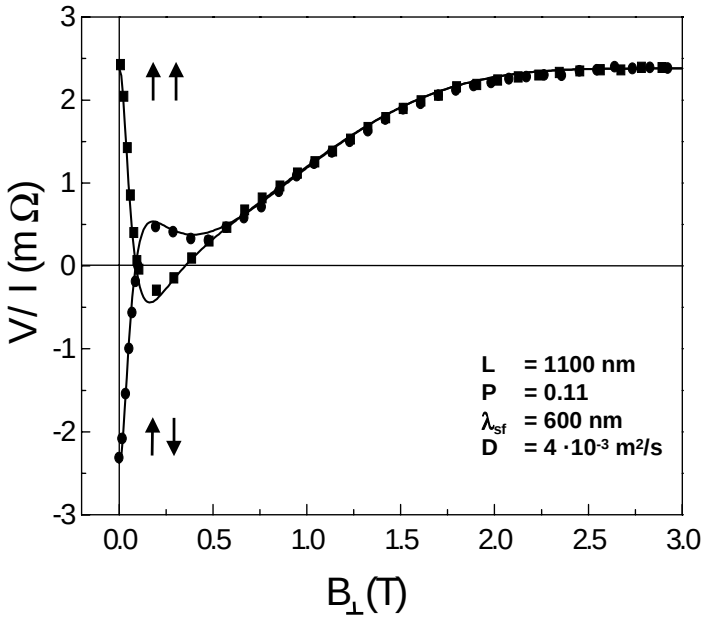

Figure 6.5: *Modulation of the output signal (V/I) due to spin precession as a function of a perpendicular magnetic field $B_\perp$, for $L = 1100$ nm. The solid squares/circles represent data taken at $T = 4.2$ K, whereas the solid lines represent the best fits based on equations 6.2 and 6.3. The arrows indicate the relative magnetization configuration (parallel/anti-parallel) of the Co electrodes.*

The data of Fig. 6.4 has been fit with eq. 6.2 and 6.3. A slightly larger $\lambda_{sf} = 500$ nm is found as compared to Fig. 6.2, which is due to the slightly higher conductivity in these samples. Using $\sigma = e^2 N(E_F) D$ and $N(E_F) = 2.4 \cdot 10^{28}$ states/eV/m^3 [21] the spin relaxation time is found to be $\tau_{sf} = 65$ ps in the Al strip at RT. This value is in fair agreement with theory [25] and consistent with the Al spin relaxation time obtained in Chapter 5. Note also that at RT about half of the momentum scattering processes is due to phonon scattering, which implies that the spin relaxation length can be maximally improved by a factor of 2 at RT, see also table 5.2.

As already visible in Fig. 6.3 and 6.4, for $B_\perp > 200$ mT an asymmetry is observed between the parallel and anti-parallel curves. This is due to the fact that the magnetization of the Co electrodes does not remain in the substrate plane. In Fig. 6.5 the measured output signal (V/I) at $T = 4.2$ K is plotted for L = 1100 nm up to $B_\perp = 3$ T, together with the calculated curve, using P, λ_{sf} and D as obtained from the best fit in Fig. 6.3. The data are in close agreement with equation 6.3, and shows a suppression of the precessional motion of the electron spin. The full magnitude of the output signal is recovered at large $B_\perp$, when $\vartheta = \pi/2$ and no precession takes place

any more.

6.4 Conclusions

An all-electrical solid-state device is fabricated which output signal is sensitive to the spin degree of freedom only. The electron spin direction can be controlled coherently and can even be reversed at liquid Helium temperatures as well as at RT. The obtained spin relaxation times in Al are in the order of 100 ps and are in agreement with theoretical predictions. The obtained tunnelling polarization P is around 10 %.

References

[1] D. D. Awschalom, D. Loss, and N. Samarth, *Semiconductor Spintronics and Quantum Computation* (Springer Verlag, Berlin, 2002).

[2] G. A. Prinz, Science **282**, 1660 (1998).

[3] S. A. Wolf, D. D. Awschalom, R. A. Buhrmann, J. M. Daughton, S. von Molnár, M. L. Roukes, A. Y. Chtchelkanova, and D. M. Treger, Science **294**, 1488 (2001).

[4] M. Johnson and R. H. Silsbee, Phys. Rev. Lett. **55**, 1790 (1985).

[5] F. J. Jedema, A. T. Filip, and B. J. van Wees, Nature **410**, 345 (2001).

[6] D. Huertas-Hernando, Y. V. Nazarov, A. Brataas, and G. E. W. Bauer, Phys. Rev. B **62**, 5700 (2000).

[7] G. Salis, Y. Kato, K. Ensslin, D. C. Driscoll, A. C. Gossard, and D. D. Awschalom, Nature **414**, 619 (2001).

[8] J. M. Kikkawa and D. D. Awschalom, Nature **397**, 139 (1999).

[9] G. Schmidt, D. Ferrand, L. W. Molenkamp, A. T. Filip, and B. J. van Wees, Phys. Rev. B **62**, R4790 (2000).

[10] E. I. Rashba, Phys Rev. B Rap. Com. **62**, R16267 (2000).

[11] A. Fert and H. Jaffrès, Phys Rev. B **64**, 184420 (2001).

[12] L. D. Jackel, R. E. Howard, E. L. Hu, D. M. Tennant, and P. Grabbe, Appl. Phys. Lett. **39**, 268 (1981).

[13] F. J. Jedema, M. S. Nijboer, A. T. Filip, and B. J. van Wees, Journal of Superconductivity **15 (1)**, 27 (2002).

[14] M. Julliere, Physics Letters **54A**, 225 (1975).

[15] R. Meservey and P. M. Tedrow, Physics Reports **238**, 173 (1994).

[16] P. LeClair, Ph.D. thesis, Eindhoven University of Technology (2002), ISBN 90-386-1989-8.

[17] P. C. van Son, H. van Kempen, and P. Wyder, Phys. Rev. Lett. **58**, 2271 (1987).

[18] M. Johnson, Phys. Rev. Lett. **70**, 2142 (1993).

[19] F. J. Jedema, M. S. Nijboer, A. T. Filip, and B. J. van Wees, submitted to Phys. Rev. B.

[20] F. J. Jedema, M. V. Costache, H. B. Heersche, J. J. A. Baselmans, and B. J. van Wees, submitted to Appl. Phys. Lett.

[21] D. A. Papaconstantopoulos, *Handbook of the band structure of elemental solids* (Plenum, New York, 1986).

[22] R. Meservey and P. M. Tedrow, Phys. Rev. Lett. **41**, 805 (1978).

[23] F. B. P. Monod, Phys. Rev. B **19**, 911 (1979).

[24] C. Grimaldi and P. Fulde, Phys. Rev. Lett. **77**, 2550 (1996).

[25] J. Fabian and S. D. Sarma, Phys. Rev. Lett. **83**, 1211 (1999).

[26] J. S. Moodera, L. R. Kinder, T. M. Wong, and R. Meservey, Phys. Rev. Lett. **74**, 3273 (1995).

[27] R. Coehoorn, *Lecture notes 'New magnetoelectronic materials and devices'* (unpublished, 1999), 3 parts.

[28] J. M. Maclaren, X.-G. Zhang, and W. H. Butler, Phys. Rev. B **56**, 11827 (1997).

[29] R. Coehoorn, private communication.

[30] M. Johnson and R. H. Silsbee, Phys. Rev. B **37**, 5312 (1988).

[31] M. Johnson and R. H. Silsbee, Phys. Rev. B **37**, 5326 (1988).